The system uranium–palladium–boron with $U_{2.5}Pd_{20.5}B_6$, a new heavy fermion compound

2010 J. Phys.: Condens. Matter 22 125601

(http://iopscience.iop.org/0953-8984/22/12/125601)

J. Phys.: Condens. Matter **22** (2010) 125601 (8pp) doi:10.1088/0953-8984/22/12/125601

The system uranium–palladium–boron with $U_{2.5}Pd_{20.5}B_6$, a new heavy fermion compound

O Sologub[1,2], P Rogl[1,5], E Bauer[3], G Hilscher[3], H Michor[3], E Royanian[3], G Giester[4] and A P Goncalves[2]

[1] Institute of Physical Chemistry, University of Vienna, A-1090 Wien, Währingerstrasse 42, Austria
[2] Departamento Química ITN/CFMCUL, E N 10, P-2686-953 Sacavém, Portugal
[3] Institute of Solid State Physics, Vienna University of Technology, A-1040 Wien, Wiedner Hauptstrasse 8-10, Austria
[4] Institute of Mineralogy and Crystallography, University of Vienna, A-1090 Wien, Althanstrasse 14, Austria

E-mail: peter.franz.rogl@univie.ac.at

Received 31 January 2010
Published 12 March 2010
Online at stacks.iop.org/JPhysCM/22/125601

Abstract

Phase equilibria in the system U–Pd–B were established at 850 °C by light optical microscopy (LOM) and x-ray powder and single crystal diffraction. Whereas in as-cast alloys only one ternary compound, τ_1-$U_{2+x}Pd_{21-x}B_6$, was found to form at $x \sim 0.5$, a further compound τ_2 with hitherto unknown structure was observed in alloys annealed at 850 °C. Due to the formation of suitable single crystals, the crystal structures of two binary compounds, UB_{12} and UPd_3 have been redetermined from high precision x-ray data. Similarly, the crystal structure of τ_1-$U_{2.5}Pd_{20.5}B_6$ was investigated by single crystal x-ray diffraction (XRD) revealing isotypism with the $Cr_{23}C_6$-type, (space group $Fm\bar{3}m$; $a = 1.1687(5)$ nm; $R_F^2 = \Sigma|F_0^2 - F_c^2|/\Sigma F_0^2 = 0.021$). τ_1-$U_{2+x}Pd_{21-x}B_6$ is a partially ordered compound where 0.37(1)U + 0.63Pd atoms randomly share the 4a site in (0, 0, 0). Whereas mutual solubility of U-borides and Pd-borides was found at 850 °C to be below 1.0 at.%, a large homogeneity region of fcc-Pd(U, B) extends into the ternary system.

$U_{2.5}Pd_{20.5}B_6$ has metallic behavior; the ground state properties are determined from a balance of the Kondo effect and the Ruderman–Kittel–Kasuya–Yosida (RKKY) interaction, revealing long range antiferromagnetic ordering below 6 K. An extraordinarily large Sommerfeld value ($\gamma > 500$ mJ mol^{-1} K^{-2}) groups $U_{2.5}Pd_{20.5}B_6$ among heavy fermion materials.

(Some figures in this article are in colour only in the electronic version)

1. Introduction

The discovery of $CePt_3Si$ ($CePt_3B$ type) as the first heavy fermion superconductor without a center of symmetry [1, 2] has spurred intensive search for a novel superconducting state in related ternary or quaternary alloy systems [3]. Although $CePt_3B$ is not superconducting above 0.4 K [4] our studies were extended to actinoid metal—platinum metal—boron systems in search for novel materials with strong electron correlations. The aims of the presented research are threefold: (i) a detailed investigation of phase relations in the system U–Pd–B, which has not been studied yet, (ii) an evaluation of the crystal structures of ternary compounds and (iii) the characterization of physical properties of novel materials.

2. Experimental details

All samples, each of a total amount of about 0.5 g, were prepared by argon arc-melting of elemental pieces of uranium

[5] Author to whom any correspondence should be addressed.

Table 1. Crystallographic data of unary and binary boundary phases of the system U–Pd–B.

Phase	Pearson symbol	Space group	Prototype	Lattice parameters (nm)			Comments
				a	*b*	*c*	
(γU)	cI2	$Im\bar{3}m$	W	0.352 4			1135.3–774.8 °C [6, 10]
(βU)	tP30	$P4_2/mnm$	βU	1.075 9		0.565 60	774.8–667.7 °C [6, 10]
(αU)	oC4	$Cmcm$	αU	0.285 37	0.586 95	0.495 48	<667.7 °C [6, 10]
(βB)	hR423	$R\bar{3}m$	βB	1.092 51		2.381 43	<2092 °C [6, 10]
(Pd)	cF4	$Fm\bar{3}m$	Cu	0.389 1			<1555 [6, 10]
UB_{12}	cF52	$Fm\bar{3}m$	UB_{12}	0.7472			<2145 °C [6, 10]
UB_4	tP20	$P4/mbm$	UB_4	7.07		3.97 5	<2495 °C [6, 10]
UB_2	hP3	$P6/mmm$	AlB_2	3.130		3.989	<2385 °C [6, 10]
UPd_3	hP16	$P6_3/mmc$	$TiNi_3$	0.576 3–0.5775		0.954 1–0.9654	<1640 °C [6, 10]
$U_{0.8}Pd_{3.2}$	cP4	$Pm\bar{3}m$	$AuCu_3$	0.406 9			<1586 °C [6, 10]
Pd_3B	oP16	$Pnma$	Fe_3C	0.546 3	0.7567	0.485 2	<1125 °C [9, 10]
Pd_5B_2	mS28	$C2/c$	Mn_5C_2	1.278 6	0.4955 $\beta = 97.03°$	0.547 2	<1077 °C [9, 10]
Pd_2B	oP6	$Pnnm$	$CaCl_2$	0.469 18	0.512 71	0.310 96	<994 °C [9, 10]

(purity >99.8 mass%), palladium wire (99.9%) and crystalline boron (98%). The U-ingots were surface cleaned in diluted HNO_3 prior to melting. For homogeneity, the samples were re-melted several times; weight losses were checked to be smaller than 0.5 mass%. A part of each alloy was wrapped in Mo-foil, sealed in an evacuated silica tube, heat-treated at 850 °C for 350 h and finally quenched by submerging the capsule in cold water. X-ray powder diffraction data from as-cast and annealed alloys were collected by employing a Guinier–Huber image plate system with monochromatic Cu Kα_1 radiation ($8° < 2\theta < 100°$). Precise lattice parameters were calculated by least squares fits to the indexed 2θ values calibrated with Ge as internal standard ($a_{Ge} = 0.5657906$ nm). Single crystals were mechanically isolated from crushed alloys. Inspection on an AXS-GADDS texture goniometer assured high crystal quality, unit cell dimensions and Laue symmetry of the specimens prior to an x-ray intensity data collection on a four-circle Nonius Kappa diffractometer equipped with a charge coupled device (CCD) area detector employing graphite monochromated Mo Kα radiation ($\lambda = 0.071\,069$ nm). Orientation matrix and unit cell parameters were derived using the program DENZO[6]. No absorption corrections were necessary because of the rather regular crystal shape and small dimensions of the investigated specimens. The structures were solved by direct methods and were refined with the SHELX-97 program [5]. Further details of sample preparation and of the various techniques of characterization, particularly for physical properties including electrical conductivity, magnetization and specific heat measurements, have been described in our previous papers [1, 3].

3. Results and discussion

3.1. The binary boundary systems

The binary system U–B was accepted in the version given in Massalski [6], the U–Pd system was taken from the investigation by Kleykamp and Kang [7, 8] and the Pd–B system used herein is from a reinvestigation by one of the authors [9]. Crystallographic data of all binary phases relevant to the U–Pd–B boundary systems are listed in table 1.

3.2. X-ray single crystal study of UB_{12} and UPd_3

During the course of investigations, suitable single crystals for the binary compounds UB_{12} and UPd_3 were isolated from ternary alloy specimens (for details see table 2). Although the atomic arrangements for both compounds were discovered about six decades ago, their crystal structures have been studied up to now only on polycrystalline samples and atom site positions have not been retrieved with high precision (for an overview of crystal data see [10]).

Single crystal x-ray intensity data for UB_{12} revealed face centered cubic symmetry without supercell formation. Structure solution by direct methods and employing difference Fourier syntheses for the boron atoms confirmed the atom arrangement, which was proposed by Bertaut and Blum [11] on the basis of steric considerations. The refinement smoothly converged to $R_F^2 = 0.013$ and structure data are summarized in table 2. The structure of UB_{12} contains two types of unfilled boron clusters: archimedian cubo-octahedra [B_{12}] and unfilled Laves CN = 12 polyhedra [B_{12}]. Examination of boron–boron distances in UB_{12} evidences that the internal cubo-octahedral B–B distances (0.1794(4) nm) are longer than the external B–B distances (0.1696(7) nm), which form the two shorter edges of the unfilled Laves polyhedra (table 3).

Structure solution and refinement of the single crystal x-ray intensity data for UPd_3 confirm isotypism with the $TiNi_3$ structure. As a check for the correct composition, refinement of the occupancy parameters for all sites revealed full occupancy within two standard deviations. Coordination polyhedra for both U1 and U2 atoms in UPd_3 are cubo-octahedra formed by six Pd1 and six Pd2 atoms. Both palladium atoms show also cubo-octahedral coordination with eight palladium and four uranium atoms as nearest neighbors. Interatomic distances are listed in table 3.

[6] Nonius Kappa CCD, Program Package COLLECT, DENZO, SCALEPACK, SORTAV, Nonius, Delft, The Netherlands.

Table 2. Crystal structure data[a] for the compounds UB_{12}, UPd_3 and τ_1-$U_{2+x}Pd_{21-x}B_6$.

Compound/parameter	UB_{12}	UPd_3	$U_{2.5}Pd_{20.5}B_6$
Nominal composition[b]	$U_{9.1}Pd_{27.3}B_{63.6}$	$U_{16.6}Pd_{72.2}B_{11.1}$	$U_2Pd_{21}B_6$
Space group	$Fm\bar{3}m$; No. 225	$P6_3/mmc$; No. 194	$Fm\bar{3}m$; No. 225
Structure type	UB_{12}	$TiNi_3$	$Cr_{23}C_6$
Formula from refinement	UB_{12}	UPd_3	$U_2(U_{0.37}Pd_{0.63})Pd_{20}B_6$
Range for data collection	$4.72 < \theta < 36.30$	$4.07 < \theta < 36.29$	$3.02 < \theta < 36.13$
Crystal size	$26 \times 26 \times 45\ \mu m^3$	$25 \times 40 \times 50\ \mu m^3$	$40 \times 57 \times 57\ \mu m^3$
a (nm)	0.747 34(3)	0.577 59(2)	1.1687(5)
c (nm)	—	0.959 16(4)	—
Reflections in refinement	$75 F_o > 4\sigma(F_o)$ of 178	$255 F_o > 4\sigma(F_o)$ of 287	$223 F_o > 4\sigma(F_o)$ of 238
Mosaicity	<0.6	<0.8	<0.4
Number of variables	6	14	15
$R_F^2 = \Sigma\lvert F_0^2\text{-}F_c^2\rvert/\Sigma F_0^2$	0.013	0.032	0.021
R_{Int}	5.4	6.3	6.6
GOF	1.12	1.181	1.186
Extinction (Zachariasen)	0.0022(4)	0.0013(3)	0.000 057(1)
M[a]; occupancy	4a (0, 0, 0); 1.00 U	2a (0, 0, 0); 1.00 U	4a (0, 0, 0); 0.367(3)U1+0.632(3)Pd1
$U_{11}^c = U_{22}$; U_{33}	0.0028(1); $U_{33} = U_{11} = U_{22}$	0.0054(2); 0.0047(3)	0.0088(2); $U_{33} = U_{11} = U_{22}$
U_{12}		0.0027(1)	
B; occupancy	48i (1/2, y, y); $y = 0.1698(3)$ 1.00 B	—	24e (x, 0, 0) $x = 0.2669(11)$ 1.00 B
U_{iso}^d	0.0034(9)		0.0133(21)
U; occupancy		2d (1/3, 2/3, 3/4); 1.00 U	8c (1/4, 1/4, 1/4); 1.00 U
$U_{11} = U_{22}$; U_{33}		0.0062(2); 0.0041(3)	0.0108(1); $U_{33} = U_{11} = U_{22}$
U_{12}		0.0041(3)	
Pd; occupancy		6g (1/2, 0, 0); 1.00 Pd	32f (x, x, x) $x = 0.3854(4)$; 1.00 Pd2
U_{11}; U_{22}; U_{33}		0.0053(2); 0.0051(3); 0.0032(4)	$U_{11} = U_{22} = U_{33} = 0.0105(1)$
U_{23}; U_{13}; U_{12}		−0.0001(1); 0.0001(1); 0.0025(1)	$U_{23} = U_{13} = U_{12} = 0.0004(1)$
Pd; occupancy		6h (x, $2x$, 1/4) $x = 0.1731(2)$; 1.00 Pd	48h (0, y, y) $y = 0.1696(3)$; 1.00 Pd3
U_{11}; U_{22}; U_{33}		0.0052(3); 0.0061(3); 0.0035(4)	0.0112(2); $U_{22} = U_{33} = 0.0115(2)$ −0.0019(8)
U_{23}			
U_{12}		0.0048(2)	
Residual electron density; max; min in (electrons nm^{-3}) × 1000	1.23; −2.19	3.03; −4.68	2.15; −1.44

[a] Crystal structure data are standardized using the program Structure Tidy [12].
[b] Nominal composition of the alloy from which a single crystal was isolated.
[c] Anisotropic atomic displacement parameters U_{ij} in (10^2 nm^2).
[d] Isotropic atomic displacement parameter U_{iso} in (10^2 nm^2).

3.3. The crystal structure of $U_{2.5}Pd_{20.5}B_6$

Single crystals of τ_1-$U_{2+x}Pd_{21-x}B_6$ were mechanically isolated from the crushed as-cast alloy with nominal composition $U_2Pd_{21}B_6$. X-ray intensity data were consistent with a face centered cubic symmetry ($a = 1.1687(5)$ nm). The absence of extinctions is consistent with the highest and centrosymmetric space group $Fm\bar{3}m$. Structure solution by direct methods yielded a metal atom arrangement corresponding to the $Cr_{23}C_6$ type. Boron atoms were unambiguously located from difference Fourier syntheses. Significantly smaller atom displacement parameters (ADPs) for palladium in site 4a (0, 0, 0) indicate a partial substitution of palladium by uranium atoms. The refinement with anisotropic ADPs for metal atoms and isotropic thermal parameters for B revealed a random occupation of the 4a site by a mix of 37% of uranium atoms and 63% of palladium atoms. The structure refinement converged smoothly to $R_{F2} = 0.021$ leaving residual electron densities of less than 3 $e^- A^{-3}$ and defined a chemical formula $U_2(U_{0.37}Pd_{0.63})Pd_{20}B_6$ in close agreement with the homogeneity region established. Structural parameters are summarized in table 2. The chemical formula is in perfect agreement with the observation of a single-phase region of small extension (∼1 at.%, for details see section 3.4) around the composition $U_{2.5}Pd_{20.5}B_6$.

A three-dimensional view of the crystal structure of $U_{2.5}Pd_{20.5}B_6$ and the coordination polyhedra of atoms, given

Table 3. Interatomic distances (nm) for UB_{12}, UPd_3 and τ_1-$U_{2+x}Pd_{21-x}B_6$.

UB_{12}		UPd_3		$U_{2.37}Pd_{20.63}B_6$	
U–24B	0.277 49(11)	U1–6Pd1	0.288 80(1)	(0.37U1 + 0.63Pd1)–12 Pd3	0.280 50(5)
B–B	0.169 6(7)	U1–6Pd2	0.295 41(5)	U2–4Pd2	0.274 27(5)
B–4B	0.179 4(4)	U2–6Pd2	0.288 86(6)	U2–12Pd3	0.320 91(2)
B–2U	0.277 49(11)	U2–6Pd1	0.292 06(1)	B1–4Pd3	0.2282(7)
		Pd1–4Pd1	0.288 80(1)	B1–4Pd2	0.235 1(8)
		Pd1–2U1	0.288 80(1)	Pd2–3B1	0.235 1(8)
		Pd1–4Pd2	0.290 46(4)	Pd2–3Pd2	0.267 66(7)
		Pd1–2U2	0.292 06(1)	Pd2–U2	0.274 27(5)
		Pd2–2Pd2	0.278 75(12)	Pd2–6Pd3	0.292 70(6)
		Pd2–2U2	0.888 6(6)	Pd3–2B1	0.228 2(7)
		Pd2–4Pd1	0.290 46(4)	Pd3–Pd3	0.265 41(7)
		Pd2–2U1	0.295 41(5)	Pd3–(0.37U1 + 0.63Pd1)	0.280 50(5)
		Pd2–2Pd2	0.298 85(11)	Pd3–4Pd3	0.280 50(5)
				Pd3–4Pd2	0.292 70(6)
				Pd3–2U2	0.320 91(2)

in figure 1, shows fragments of columns which are formed by empty cubes [$Pd2_8$] sharing two faces along the coordinate axes with tetragonal antiprisms B[$Pd3_4Pd2_4$]. Empty cubes are formed by eight Pd2 atoms around the vacant Wyckoff site 4b (1/2, 1/2, 1/2) and correspondingly are situated at the center of the unit cell and centers of its edges. The fragments are interconnected by cubo-octahedra ($U1_{0.37}Pd1_{0.63}$)[$Pd3_{12}$], which can be found on the unit cell vertices and centers of its faces. Cubo-octahedra contribute squared faces to the tetragonal antiprisms whereas triangular faces are shared with Friauf polyhedra of U2 which are composed of 16 atoms U2[$Pd2_4Pd3_{12}$]. Atoms Pd2 and Pd3 are surrounded by 13 and 14 next-nearest neighboring atoms, respectively. Interatomic distances agree well with the metallic radii of pure elements (table 3).

It should be noted that a recent report on the single-phase region of isotypic $Ce_{2+x}Pd_{21-x}Si_6$ ($0 \leqslant x \leqslant 1$, at 800 °C) [13] revealed a similar exchange of Ce/Pd in the Wyckoff site 4a i.e. a random replacement among an f-electron element and a transition element from the platinum metal group. With respect to data collected [14, 15] on the formation and metal site preferences in τ-borides, the crystal structure of $U_{2+x}Pd_{21-x}B_6$ belongs to the branch where the more electropositive and larger U-atom acts as a stabilizer of the $Cr_{23}C_6$ type and occupies the 8c and partially the 4a atomic sites in the parent structure. For the elements with smaller differences in electronegativity and size, the substitution is realized preferably on the framework sites 48h and 32f.

3.4. Phase relations at 850 °C

Phase equilibria in the U–Pd–B system at $T = 850$ °C are characterized by the formation of two palladium-rich compounds, τ_1-$U_{2+x}Pd_{21-x}B_6$ ($x \sim 0.5$) and a compound τ_2 with unknown structure, which was only observed in annealed alloys within the compositional range 15–20U60–70Pd25–10B (in at.%). In order to document the equilibria experimentally derived, nominal compositions and phase analysis of selected alloys are summarized in table 4. It should be noted that from lattice parameter variation τ_1-$U_{2+x}Pd_{21-x}B_6$ exhibits only a small homogeneity region of about 1 at.% centered around the composition $U_{2.5}Pd_{20.5}B_6$, which forms congruently from the melt and remains in equilibrium at $T = 850$ °C with four binary phases, Pd_2B_5, $U_{0.8}Pd_{3.2}$, UPd_3 and UB_4.

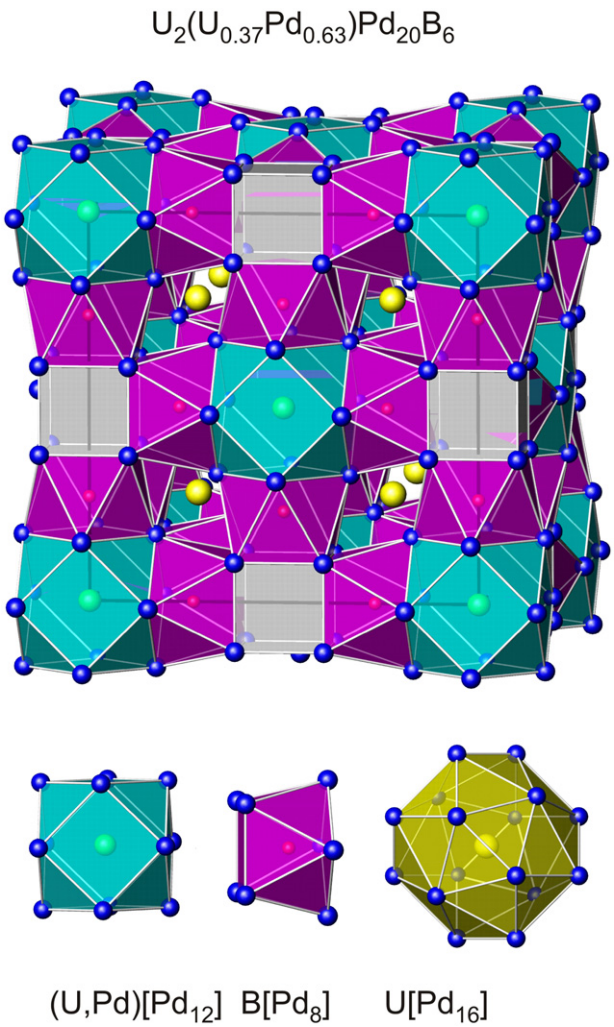

Figure 1. Three-dimensional view of the crystal structure of $U_{2+x}Pd_{21-x}B_6$ and coordination polyhedra around atoms (U, Pd), B and U (for details see the text and tables 2 and 3).

Binary compounds exhibit rather small mutual solubility for the third component, i.e. generally are smaller than 1 at.%

Table 4. Phase relations and crystallographic data of U–Pd–B alloys annealed at 850 °C.

No.	Nominal composition U–Pd–B (at.%)	Heat treatment (°C)	X-ray phase analysis	Space group	Structure type	Lattice parameters in nm		
						a	*b*	*c*
1	16.6–66.7–16.6	850	UPd_3	$P6_3/mmc$	$TiNi_3$	0.5765(4)	0.9596(5)	
			τ_2	Unknown	—			
			UB_4	$P4/mbm$	UB_4	0.7078(5)		0.3980(3)
2	20–60–20	850	UPd_3	$P6_3/mmc$	$TiNi_3$	0.5768(3)		0.9595(6)
			τ_2	Unknown	—			
			UB_4	$P4/mbm$	UB_4	0.7085(4)		0.3980(3)
3	6.9–72.4–20.6	850	Pd_5B_2	$C2/c$	Mn_5C_2	1.2807(7)	0.4942(3)	0.5459(4)
					—		$\beta = 96.9(1)°$	
			$U_{0.8}Pd_{3.2}$	$Pm\bar{3}m$	$AuCu_3$	0.4081(3)		
			$U_{2.5}Pd_{20.5}B_6$	$Fm\bar{3}m$	$Cr_{23}C_6$	1.1651(8)		
4	9.2–68.3–22.5	850	$U_{2.5}Pd_{20.5}B_6$	$Fm\bar{3}m$	$Cr_{23}C_6$	1.1675(4)		
			UB_4	$P4/mbm$	UB_4	0.7080(6)		0.3982(3)
			Pd_5B_2	$C2/c$	Mn_5C_2			
5	25–50–25	850	UB_4	$P4/mbm$	UB_4	0.7075(4)		0.3980(3)
			UPd_3	$P6_3/mmc$	$TiNi_3$	0.5769(4)		0.9630(5)
6	5.3–61.2–31.6	850	$U_{2.5}Pd_{20.5}B_6$	$Fm\bar{3}m$	$Cr_{23}C_6$	1.1652(3)		
			Pd_5B_2	$C2/c$	Mn_5C_2	1.2796(8)	0.4946(4)	0.5476(5)
					—		$\beta = 97.0(1)°$	
			UB_4	$P4/mbm$	UB_4	0.7037(6)		0.3967(4)
7	16.6–16.6–66.7	850	UB_4	$P4/mbm$	UB_4	0.7087(3)		0.3989(2)
			$U_{2.5}Pd_{20.5}B_6$	$Fm\bar{3}m$	$Cr_{23}C_6$	1.1662(3)		
			τ_2	Unknown				
8	22.2–5.5–72.3	850	UPd_3 (traces)	$P6_3/mmc$	$TiNi_3$	0.5768(7)		0.9543(9)
			UB_4	$P4/mbm$	UB_4	0.7073(3)		0.3979(3)
			UB_2	$P6/mmm$	AlB_2	0.3129(2)		0.3987(2)
10	9.1–27.2–63.6	850	Pd_5B_2	$C2/c$	Mn_5C_2	1.2848(7)	0.4991(5)	0.5477(6)
					—		$\beta = 96.97(1)°$	
			UB_{12}	$Fm\bar{3}m$	UB_{12}	0.7469(3)		
			UB_4	$P4/mbm$	UB_4	0.7074(3)		0.3908(3)
11	16.7–61.1–22.2	850	UPd_3	$P6_3/mmc$	$TiNi_3$	0.5765(3)		0.9596(5)
			τ_2	Unknown	—			
			UB_4	$P4/mbm$	UB_4	0.7078(4)		0.3980(3)
12	16.7–72.2–11.1	850	UPd_3	$P6_3/mmc$	$TiNi_3$	0.5775(3)		0.9580(4)
			$U_{2.5}Pd_{20.5}B_6$	$Fm\bar{3}m$	$Cr_{23}C_6$	1.1660(3)		
			τ_2	Unknown	—	—		
		As-cast	UPd_3	$P6_3/mmc$	$TiNi_3$	0.5773(4)		0.9599(5)
			$U_{2.5}Pd_{20.5}B_6$	$Fm\bar{3}m$	$Cr_{23}C_6$	1.1687(4)		
13	18.2–27.2–54.6	850	UB_4	$P4/mbm$	UB_4	0.7075(4)		0.3979(3)
			UPd_3	$P6_3/mmc$	$TiNi_3$	0.5773(3)		0.9588(5)
			τ_2	Unknown	—	—		
14	14–72–14	850	UPd_3	$P6_3/mmc$	$TiNi_3$	0.5773(4)		0.9585(6)
			$U_{2.5}Pd_{20.5}B_6$	$Fm\bar{3}m$	$Cr_{23}C_6$	1.158(1)		
			τ_2	Unknown	—	—		
15	45–5–50	850	UB_4	$P4/mbm$	UB_4	0.7070(4)		0.3978(2)
			Pd_2B	$Pnnm$	$CaCl_2$	1.2805(9)	0.4966(4)	0.5475(7)
					—		$\beta = 97.0(1)°$	
			UB_{12}	$Fm\bar{3}m$	UB_{12}	0.7465(4)		
16	25–25–50	850	UB_2	$P6/mmm$	AlB_2	0.3132(3)		0.3986(3)
			UB_4	$P4/mbm$	UB_4	0.7076(4)		0.3980(3)
			UPd_3	$P6_3/mmc$	$TiNi_3$	0.5768(3)		0.9635(5)
17	40–20–40	850	UB_2	$P6/mmm$	AlB_2	0.3131(3)		0.3985(3)
			U	$Cmcm$	αU	0.285(1)	0.589(1)	0.495(1)
			UPd_3	$P6_3/mmc$	$TiNi_3$	0.5772(3)		0.9589(5)
18	40–40–20	850	UB_2	$P6/mmm$	AlB_2	0.3132(3)		0.3986(4)
			U	$Cmcm$	αU	0.2852(6)	0.5897(9)	0.4962(7)
			UPd_3	$P6_3/mmc$	$TiNi_3$	0.5775(3)		0.9587(6)

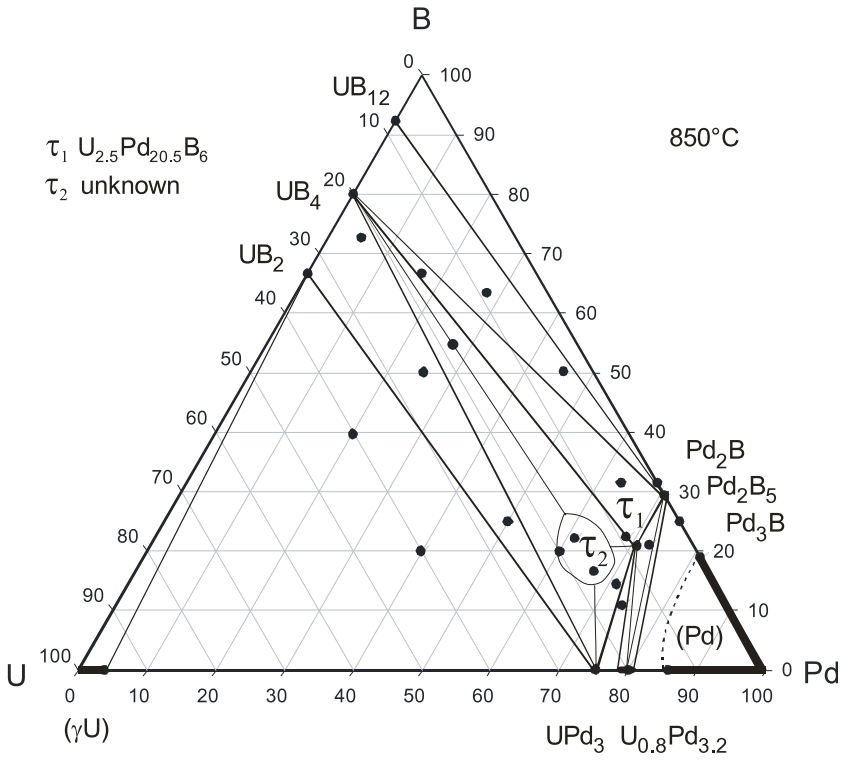

Figure 2. System U–Pd–B; isothermal section at 850 °C.

as established from x-ray powder diffraction data analysis of multiphase alloys. In consistency with the large binary solubilities of both U in (Pd) and B in (Pd), the phase field of the cubic face centered (Pd) solid solution (ss) extends far into the ternary system. The Pd-rich corner and the precise boundary of ss-(Pd), however, were not investigated. The isothermal section defined at $T = 850\,^{\circ}\mathrm{C}$ is shown in figure 2.

3.5. Physical properties of heavy fermion $U_{2.5}Pd_{20.5}B_6$

For physical property measurements a sample $U_{2.5}Pd_{20.5}B_6$ was used. The specific heat of $U_{2.5}Pd_{20.5}B_6$, as shown in figure 3, reveals a pronounced anomaly at about 6 K signaling the onset of long range bulk magnetic order. Long range magnetic order due to RKKY interactions follows from a U–Pd interplay as direct uranium distances are rather large ($d_{\mathrm{U-U}} = 0.584\,35$ nm). The inset of figure 3 shows low temperature details. In order to qualitatively account for the ordered region of $U_{2.5}Pd_{20.5}B_6$, a model developed by Continentino in [16] is applied, yielding an analytic expression regarding the temperature dependent specific heat:

$$C_{\mathrm{mag}} = g\Delta^{7/2}T^{1/2}\exp\left(-\frac{\Delta}{T}\right)\left[1+\frac{39}{20}\left(\frac{T}{\Delta}\right)+\frac{51}{32}\left(\frac{T}{\Delta}\right)^2\right]. \quad (1)$$

This expression is based on antiferromagnetic magnons with a dispersion relation given by $\omega = \sqrt{\Delta^2 + D^2k^2}$, where Δ is the spin wave gap and D is the spin wave velocity. Applying equation (1) to the experimental data yields a spin wave gap $\Delta = 3.2$ K, reasonable with respect to the magnetic phase transition temperature of about 6 K as well as a Sommerfeld

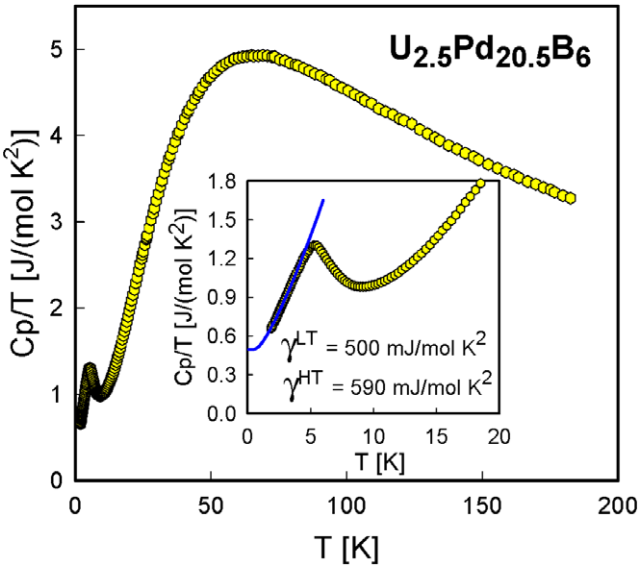

Figure 3. Temperature dependent specific heat C_p of $U_{2.5}Pd_{20.5}B_6$, plotted as C_p/T versus T and a close-up for the low temperature region in the inset. The solid line in the inset is a least squares fit as explained in the text.

value $\gamma = 500$ mJ mol^{-1} K^{-2}. Results of this fit are shown as a solid line in the inset of figure 3. Note that a standard evaluation of the Sommerfeld constant reveals $\gamma = 590$ mJ mol^{-1} K^{-2}. These values clearly group $U_{2.5}Pd_{20.5}B_6$ among heavy fermion systems.

Magnetization measurements in external magnetic fields up to 6 T were carried out in a Cryogenic SQUID

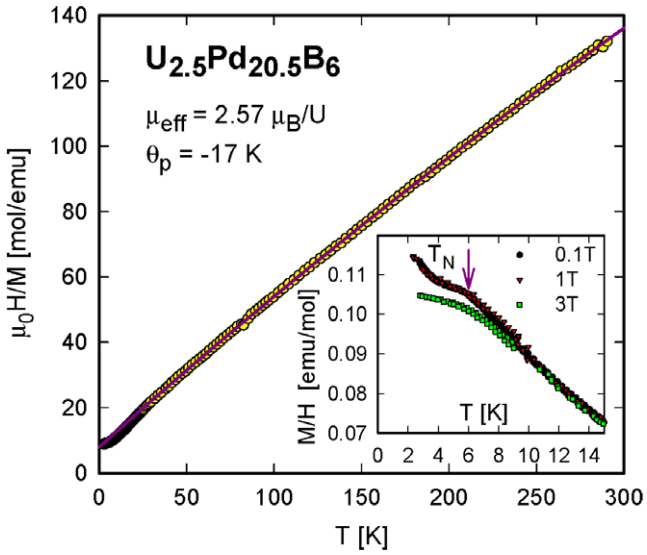

Figure 4. Temperature dependent magnetic susceptibility χ of $U_{2.5}Pd_{20.5}B_6$, plotted as $1/\chi$ versus T. The solid line is a least squares fit according to the Curie–Weiss law. The inset shows the susceptibility as a function of temperature for various fields.

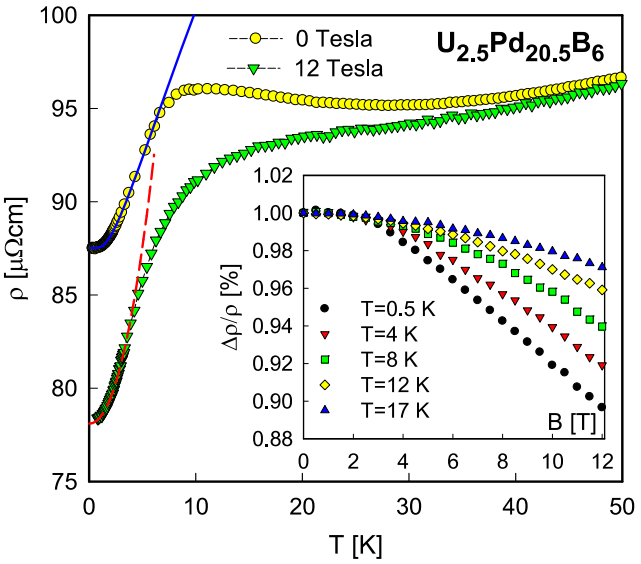

Figure 5. Temperature dependent resistivity ρ of $U_{2.5}Pd_{20.5}B_6$ shown for magnetic fields of 0 and 12 T. The solid lines are least squares fits as explained in the text. Magnetoresistivity ρ(B) of $U_{2.5}Pd_{20.5}B_6$ shown for various temperatures 0.5 K $< T <$ 17 K.

magnetometer. Main results on susceptibility, χ, and magnetization, M, of $U_{2.5}Pd_{20.5}B_6$ are summarized in figure 4. The inset in figure 4 reveals a broad kink at about 6 K for 0.1 and 1 T, which is washed out and shifted to lower temperatures for 3 T. This is indicative of antiferromagnetic order, in agreement with the analysis of the specific heat data in terms of antiferromagnetic magnons. The main body of the figure displays the magnetic susceptibility χ plotted as $1/\chi$ versus temperature, taken at an external field of 1 T. The paramagnetic state can be accounted for in terms of a modified Curie–Weiss law, i.e. $\chi = \chi_0 + C/(T - \theta_p)$, where $\chi_0 = 8 \times 10^{-4}$ emu mol^{-1} represents a temperature independent susceptibility, C is the Curie constant yielding an effective moment $\mu_{eff} = 2.57\ \mu_B$/U (=4.06 μ_B/f.u.) and $\theta_p = -17$ K is the paramagnetic Curie temperature. The effective magnetic moment observed strongly deviates from the $^4I_{9/2}$ ground state of an ideal U^{3+} ion ($\mu_{eff} = 3.78\ \mu_B$), which hints towards a hybridized $5f^{3-x}6d^x$ electronic configuration of the U ions and the negative Curie–Weiss temperature indicates antiferromagnetic interaction. Crystalline electric field (CEF) effects are unlikely to play a significant role in $U_{2.5}Pd_{20.5}B_6$ since $1/\chi$ reveals a lack of a pronounced curvature. Isothermal magnetization measurements in the temperature range from 2 to 30 K (not shown here) do not display ferro- or ferrimagnetic order in terms of Arrott plots. The scaling of the magnetic isotherms as a function of the reduced external field (H/T) with respect to temperature deviates significantly from that of a paramagnetic ground state and is typical for antiferromagnetic order. Consequently, antiferromagnetic ordering can be concluded for $U_{2.5}Pd_{20.5}B_6$ in accordance with low temperature specific heat results.

We have studied the electrical resistivity ρ of $U_{2.5}Pd_{20.5}B_6$ from 0.3 K to room temperature as a function of several magnetic fields up to 12 T. Figure 5 shows $\rho(T)$ for 0 and 12 T. With a shallow minimum around 25 K, which is particularly pronounced in the absence of a magnetic field, and with a steep drop below about 10 K, $\rho(T)$ does not follow a simple metallic behavior, rather suggesting the presence of Kondo interaction and long range magnetic order. The inset of figure 5 displays the isothermal magnetoresistance, $\Delta\rho/\rho$, of $U_{2.5}Pd_{20.5}B_6$ for temperatures below and above the magnetic phase transition. In both ranges negative values are observed for $\Delta\rho/\rho$. It is well known that the Kondo effect is responsible for a large and negative magnetoresistance of the material; its field dependence is entirely governed by a characteristic field H^* which is proportional to the characteristic Kondo temperature T_K.

A qualitative and quantitative description of the temperature dependent electrical resistivity can be accomplished in terms of the above indicated model of Continentino [16], revealing

$$\rho = \rho_0 + A\Delta^{3/2}T^{1/2}\exp\left(-\frac{\Delta}{T}\right)\left[1 + \frac{2}{3}\left(\frac{T}{\Delta}\right) + \frac{2}{5}\left(\frac{T}{\Delta}\right)^2\right]. \quad (2)$$

Here, electrons are scattered on antiferromagnetic magnons with a dispersion relation already introduced for the discussion of the specific heat data. Note that $A \propto 1/D^3 \propto \Gamma^3$; Γ is an effective coupling between the U ions. Applying equation (2) to the experimental data (solid line, figure 4) yields a spin wave gap $\Delta = 4$ K, in reasonable agreement with the heat capacity results. ρ_0 is the residual resistivity. The application of an external field of 12 T obviously quenches the antiferromagnetism of $U_{2.5}Pd_{20.5}B_6$ and recovers a Fermi-liquid ground state reflected from the T^2 behavior of the low temperature resistivity (dashed line, figure 5).

4. Summary

Phase equilibria in the system U–Pd–B were established in an isothermal section at 850 °C. The compound τ_1-$U_{2.5}Pd_{20.5}B_6$ was found to form congruently and to be stable in the investigated temperature range. A compound τ_2 with unknown structure was observed to form after annealing at 850 °C in the ~$U_{15-20}Pd_{60-70}B_{25-10}$ compositional region. The crystal structure of τ_1-$U_{2+x}Pd_{21-x}B_6$, derived from Kappa CCD single crystal x-ray data, revealed a random occupation of the 4a site by 37% of U and 63% of Pd atoms, yielding a formula $U_2(U_{0.37}Pd_{0.63})Pd_{20}B_6$. Precise atom positions were also determined for the binary compounds UB_{12} and UPd_3 from single crystal x-ray data. Measurements of thermodynamic properties (specific heat and magnetic susceptibility) as well as electrical resistivity characterize $U_{2.5}Pd_{20.5}B_6$ as an antiferromagnet with $T_N \sim 6$ K where a gap of the order of 3–4 K opens in the spin wave dispersion relation. A pronounced minimum in the temperature dependent resistivity around 30 K refers to the presence of the Kondo effect. The effective magnetic moment deduced is well below that expected for a U^{3+} ion, possibly as a consequence of Kondo screening. A very large Sommerfeld value, of the order of 500 mJ mol^{-1} K^{-2}, is thought to originate from the mutual balance of the RKKY interaction and the Kondo effect, clearly classifying $U_{2.5}Pd_{20.5}B_6$ as a heavy fermion system.

Acknowledgments

This research was supported by the Austrian National Science Foundation FWF projects M1067-N20 and 18054. PR and OS are grateful for STMs within the action COST-P16 at ITN in Sacavem, Portugal and at IPC in Vienna, Austria, respectively.

References

[1] Bauer E, Hilscher G, Michor H, Paul C, Scheidt E W, Grybanov A, Seropegin Yu, Noël H, Sigrist M and Rogl P 2004 *Phys. Rev. Lett.* **92** 027003
[2] Tursina A I, Gribanov A V, Noël H, Rogl P and Seropegin Yu D 2004 *J Alloys Compounds* **373** 239–41
[3] Bauer E, Hilscher G, Kaldarar H, Michor H, Scheidt E W, Rogl P, Gribanov A and Seropegin Yu 2007 *J. Magn. Magn. Mater.* **310** e73–5
[4] Lackner R, Sieberer M, Michor H, Hilscher G, Bauer E, Salamakha P, Sologub O and Hiebl K 2005 *J. Phys.: Condens. Matter* **17** S905–10
[5] Sheldrick G M 1997 *SHELXS-97, Program for Crystal Structure Refinement* University of Göttingen, Germany
[6] Massalski T B 1990 *Binary Alloy Phase Diagrams* 2nd edn (Materials Park, OH: ASM International)
[7] Kleykamp H and Kang S G 1991 *Z. Met.kd.* **82** 544–52
[8] Kleykamp H and Kang S G 1996 *J. Nucl. Mater.* **230** 280–6
[9] Rogl P 1998 The Pd–B–C system *Phase Diagrams of Ternary Metal–Boron–Carbon Systems* ed G Effenberg (Materials Park, OH: ASM International) pp 234–9
[10] Villars P and Calvert L D 1991 *Pearson's Handbook of Crystallographic Data for Intermetallic Phases* 2nd edn (Materials Park, OH: ASM International)
[11] Bertaut F and Blum P 1949 *C. R. Acad. Sci., Paris* **229** 111
[12] Parthé E, Gelato L, Chabot B, Penzo M, Censual K and Gladyshevskii R 1994 *TYPIX—Standardized Data and Crystal Chemical Characterization of Inorganic Structure Types* (Berlin: Springer)
[13] Lipatov A, Gribanov A, Grytsiv A, Rogl P, Murashova E, Seropegin Yu, Giester G and Kalmykov K 2009 *J. Solid State Chem.* **182** 2497–509
[14] Rogl P 1991 Existence and crystal chemistry of borides *Inorganic Reactions and Methods* vol 13, ed J J Zuckerman and A P Hagen (New York: VCH) pp 85–167
[15] Sologub O, Rogl P and Giester G 2010 *Intermetallics* **18** 694–701
[16] Continentino M, de Medeiros S N, Orlando M T D, Fontes M B and Baggio-Saitovitch E M 2001 *Phys. Rev.* B **64** 012404